



Numerical simulation study on ventilation and harmful gas diffusion during the construction period of shafts

Q. Shi¹ · J. Chai¹ · J. Cao¹ · T. Yang¹

Received: 23 December 2022 / Revised: 15 October 2023 / Accepted: 24 October 2023 / Published online: 22 November 2023

© The Author(s) under exclusive licence to Iranian Society of Environmentalists (IRSEN) and Science and Research Branch, Islamic Azad University 2023

Abstract

In the process of excavating the shaft, blasting will generate a large amount of CO, which will pollute the environment inside the shaft and jeopardize the health of the construction workers. In this study, the theoretical equation of CO distribution inside the shaft during the construction period is derived based on the diluted ventilation model. The ventilation process in the shaft under different working conditions was numerically simulated. And the grid convergence index method was used to study the independence of the grid to ensure the accuracy of the numerical simulation. The selection of the location of the duct is the main factor affecting the distribution of the flow field in the shaft. The distance between the outlet of the duct and the working face of the shaft is the main factor affecting the dilution of CO in the shaft. The flow rate of the jet ejected from the outlet of the duct is the main factor influencing the movement rate of the CO peak. The distribution functions of hazardous gases in the shaft with space and time when the shaft is ventilated by forced ventilation are derived. Based on the diameter of the shaft and the ventilation volume, the formula for estimating the ventilation time required for shaft construction was constructed. The accuracy of the formula was verified by the actual projects. The optimized ventilation measures by using the results of this study can effectively improve the construction environment in the shaft, which has certain significance for similar projects.

Keywords Shaft under construction · Forced ventilation · Environment in the shaft · Ventilation effect · Ventilation time

Introduction

Shafts have a wide range of applications in hydraulic engineering. Whether as a permanent ventilation shaft, a regulating shaft for a diversion tunnel, or a multi-sectional construction using a shaft to shorten the construction period, the excavation of a shaft is indispensable (Shao et al. 2016; Zhang et al. 2018). The current main method of shaft excavation is the drill and blast method (Tang et al. 2018; Tangjarusritatororn et al. 2022). Regardless of the excavation method, harmful gases are generated by blasting, which pollute the environment of the tunnel and pose a threat to the lives and health of the construction workers (Wang et al.

2009; Wang et al. 2011; Liu et al. 2014; Sousa and Einstein 2021). According to a survey conducted by relevant organizations in China, the number of respiratory diseases caused by the nature of occupation accounted for 99.7% of the total respiratory morbidity in the country in 2018 (Xie et al. 2021). At present, the ventilation during the construction period of the shaft is based on forced ventilation, which is used to wash down the gun smoke and discharge it along the shaft by jet of fans. Therefore, it is necessary to study the ventilation during the construction period of the shaft to ensure the safety of the construction personnel and the efficiency of the construction.

In the process of tunnel construction, there are many factors affecting the ventilation. For different influencing factors, different scholars have done corresponding research. Zhou et al. (2020) proposed an empirical formula applicable to the calculation of the required air supply volume for pressurized ventilation. Nan et al. (2015) as well as Huang et al. (2011) studied the distance between the duct outlet and the working face and derived a semi-empirical formula for determining the effective length of the airflow. Parra et al.

Editorial responsibility: Mohamed F. Yassin.

✉ J. Chai
jrchai@xaut.edu.cn

¹ State Key Laboratory of Eco-Hydraulics in Northwest Arid Region of China, Xi'an University of Technology, Xi'an 710048, China



(2006) studied the ventilation efficiency of different ventilation systems. Wang et al. (2012) studied the horizontal deflection angle of fans in ventilation systems and determined the optimal deflection angle of jet fans in curved tunnels. Hasheminasab et al. (2019) studied the ventilation effect of auxiliary ventilation system and also studied the effect of different factors on ventilation. Torano et al. (2009) studied the local tunnel ventilation system and further optimized the tunnel ventilation system based on the results of the study. It can be seen that scholars have studied the single-headed tunnels in depth and analyzed the influence of different factors on ventilation during the construction period.

The ventilation process of shafts, an integral part of tunneling, has also been further studied by many scholars (Shao et al. 2016; Liu et al. 2019; Peng et al. 2021; Wang et al. 2022). Kazakov et al. (2015) studied the pattern of natural ventilation in the shaft after the fan stops in the vertical mine and proposed a mathematical model capable of predicting the intensity of natural ventilation. Semin and Levin (2021) conducted a theoretical study of the conditions for the occurrence of return air in the shaft and identified criteria for quantitative analysis of the flow structure in the shaft. A detailed study of the effect of the cross-section of the shaft on the natural smoke exhaust from the tunnel was conducted by Xie et al. (2018). Shao et al. (2016) conducted a simulation study of different ventilation schemes for a hydroelectric power plant sloping cavern complex. By analyzing the flow field in the tunnel, it was demonstrated that the advance construction of shafts can greatly improve the ventilation conditions in the tunnel. Szlęzak et al. (2017) studied the ventilation of an underground mine tunnel complex using shafts and optimized the design of the ventilation network. Guo et al. (2021) analyzed different cases to determine the optimal position of shafts in the tunnel when using them for ventilation. Liu et al. (2018) studied the effect of air pressure difference caused by deep shafts on ventilation during shaft construction and proposed a mathematical model of two-phase flow considering the effect of pressure difference and validated it. Zhang et al. (2019) studied the effect of shaft depth on its natural ventilation and concluded that it is more affected by depth when the depth is less than 250 m.

It can be seen that the research on ventilation of shafts is mostly focused on the ventilation of shafts during the operation period after they are built or the effect of shafts on the ventilation of the whole underground building construction period. During the excavation of the shaft, due to its longitudinal construction characteristics, ventilation is more difficult compared to the ventilation of a tunnel on a single horizontal plane. It is difficult to achieve the optimal ventilation efficiency only through the previous construction experience. In the process of shaft construction, various factors

have an impact on the ventilation effect, such as the flow rate of air ejected from the duct, the diameter of the shaft, the location of the duct arrangement, the distance between the outlet of the duct and the working face, etc. Therefore, this study focuses on the ventilation process during the construction period of the shaft. By studying the flow and concentration fields of hazardous gases in the shaft, the mechanism of the influence from different factors on the construction ventilation is obtained. Thus, the ventilation system during the construction period of the shaft can be optimized, and the ventilation efficiency can be improved.

Materials and methods

Materials

In this study, the ventilation model of a shaft under different working conditions was investigated. The medium within the model is CO and air. The effects of four factors, namely, the location of the duct, the distance between the outlet of the duct and the working face, the air velocity, and the diameter of the shaft, on the ventilation effect were investigated separately. The shaft model has a length of 500 m and a diameter of 5.5 m. The ventilation during the construction period of the shaft is based on forced ventilation. The data for validating the model were used from the experimental results of Rajaratnam et al. (Nan, 2015). The data of the relevant engineering examples were adopted from the field data of two actual projects, the Datai Shaft of the Wushaoling Tunnel (Li and Luo, 2005) in China and the No. 2 Shaft of the Qinling-ZhongNan Mountain highway tunnel (Xu, 2008) in China. The software used for numerical simulation calculations is FLUENT.

Methods

In this study, the theoretical distribution function of CO concentration in the shaft during ventilation is firstly derived by means of theoretical analysis, and then numerical simulation is used for further study. Different working conditions are classified according to different influencing factors. The grid error is analyzed by using the grid convergence index method. Model validation is carried out by comparing with the experimental data obtained by Rajaratnam et al. (Nan, 2015). The flow field distribution is analyzed for different working conditions. The extent of influence from different factors on the flow field in the shaft is explored. The CO concentration field in the shaft under different working conditions is



quantitatively analyzed. The effect of different factors on the CO concentration field in the shaft is then investigated. The distribution function of CO in the shaft is fitted by combining the results of theoretical analysis and numerical simulation, and then the formula for calculating the ventilation time is derived. Finally, the formula for calculating the ventilation time is verified by actual engineering data.

Theoretical derivation of CO distribution equation inside the shaft

When forced ventilation is used in shafts, there are both jet and backflow in the shaft. As shown in Fig. 1, in the area between the outlet of the duct and the working face, the two flow regimes are mixed with each other, and the flow distribution is complex. Therefore, the distribution of CO concentration in this area is analyzed separately. The area between the outlet of the duct and the working face is defined as Area I, and the area between the outlet of the duct and the shaft outlet is defined as Area II. Initial conditions in the shaft: The CO concentration in Area I is C_0 , the CO concentration in Area II is 0, and the ventilation volume per unit time in the duct is ΔQ . Some basic assumptions are also made: (1) The airflow ejected from the duct is evenly distributed at the outlet of the duct; (2) the CO in Area I is uniformly distributed; and (3) the wall of the shaft is insulated.

Based on the research results of Yang et al. (2000), the theoretical derivation of the distribution function for CO in a shaft with forced ventilation was carried out. Considering only the convection process between the gases, the duct shoots ΔQ of fresh air into Area I per unit time Δt and mixes with the CO in Area I uniformly. The concentration

of CO in Area I is C_n at this time. Therefore, after t time ($n \Delta t$) of ventilation, the concentration of CO in Area I can be obtained by Eq. (1).

$$C = \lim_{n \rightarrow \infty} C_n = \lim_{n \rightarrow \infty} C_0 \left(\frac{SL_0}{SL_0 + Q\Delta t} \right)^n = \lim_{\Delta t \rightarrow 0} C_0 \left(\frac{SL_0}{SL_0 + Q\Delta t} \right)^{t/\Delta t} = C_0 e^{-Qt/SL_0} \tag{1}$$

Since the gas is assumed to be incompressible, a mixture of ΔQ also flows into Area II. In the process of ventilation, the gas mixture is continuously flowing toward the outlet of the shaft for a maximum distance $z_{\max} = (Qt + SL_0)/S$. When $L_0 < z < z_{\max}$, the concentration of CO can be obtained by Eq. (2); when $z > z_{\max}$, the concentration of CO is 0. Therefore, the CO concentration in the shaft during ventilation can be expressed by Eq. (3).

$$C(z, t) = C_0 e^{-\frac{Qt - (z - L_0) \times S / Ql}{SL_0}} = C_0 e^{\frac{z}{L_0} - \frac{Qt}{SL_0} - 1} \tag{2}$$

$$C(z, t) = \begin{cases} 0 & z > z_{\max} \\ C_0 e^{-\frac{Qt}{SL_0}} & z < L_0 \\ C_0 e^{\frac{z}{L_0} - \frac{Qt}{SL_0} - 1} & L_0 < z < z_{\max} \end{cases} \tag{3}$$

where C is the concentration of CO in the shaft (mg/m^3); C_0 is the initial concentration of CO (mg/m^3); t is the ventilation time (s); z is the distance between the CO calculation point and the working face of the shaft (m); L_0 is the length of Area I (m), i.e., the distance between the outlet of the duct and the working face of the shaft; and S is the area of the working face of the shaft (m^2).

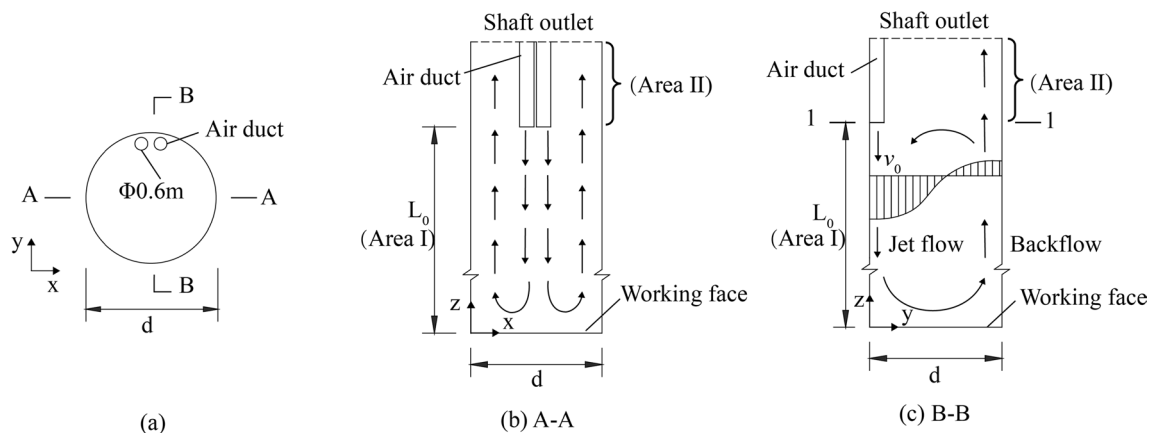


Fig. 1 Cross-section and longitudinal section of the shaft

Mathematical methods and model analysis

Governing equation

In simulating the ventilation process in the shaft during the construction period, the following basic assumptions are made:

- (1) The air in the shaft is a continuous medium and incompressible;
- (2) The airflow at the outlet of the duct is uniformly distributed, with the emitted airflow perpendicular to the duct boundary and isothermal;
- (3) The heat dissipation in the airflow process is not considered, and the air leakage from the duct is not considered;
- (4) The corresponding shaft model is simplified. The remaining mechanical equipment in the shaft and the obstacles that may interfere with the flow field are ignored.

When forced ventilation is used, the flow field inside the shaft will inevitably have insufficient flow development and unclear flow conditions. At the same time, the doping of jet, reflux, and stagnation in the flow field makes the distribution complex. Although the Standard k - ε model has a simple form and high computational efficiency, it cannot better reflect the anisotropy of bending wall flow. During the process of ventilation, the airflow direction changes after passing through the working face of the shaft. The turning of the airflow is too large, which will affect the calculation accuracy of the model. The RNG k - ε model takes the influence of eddy currents into account and is more accurate for small eddy currents than the Standard k - ε model. The Realizable k - ε model, on the other hand, takes the rotation and curvature-related flows into account more fully. Therefore, it is more suitable for the flow characteristics of the shaft outlet in theory. Many scholars have also demonstrated that the Realizable k - ε model is better in the calculation compared to the other two models (Zhang et al. 2019; Zhang et al. 2020, Chang 2020). The Realizable k - ε model is chosen for the study by combining all the above factors.

The k and ε equations in the Realizable k - ε model can be expressed by Eqs. (4) and (5), respectively (Chang 2020):

$$\frac{\partial}{\partial t}(\rho k) + \frac{\partial}{\partial x_j}(\rho k u_j) = \frac{\partial}{\partial x_j} \left[\left(\mu + \frac{\mu_t}{\sigma_k} \right) \frac{\partial k}{\partial x_j} \right] + G_k + G_b - \rho \varepsilon - Y_M + S_k \quad (4)$$

$$\begin{aligned} \frac{\partial}{\partial t}(\rho \varepsilon) + \frac{\partial}{\partial x_j}(\rho \varepsilon u_j) = & \frac{\partial}{\partial x_j} \left[\left(\mu + \frac{\mu_t}{\sigma_\varepsilon} \right) \frac{\partial \varepsilon}{\partial x_j} \right] \\ & + \rho C_1 S \varepsilon - \rho C_2 \frac{\varepsilon^2}{k + \sqrt{\nu \varepsilon}} \\ & + C_{1\varepsilon} \frac{\varepsilon}{k} C_{3\varepsilon} G_b + S_\varepsilon \end{aligned} \quad (5)$$

where

$$C_1 = \max \left[0.43, \frac{\eta}{\eta + 5} \right], \quad \eta = S \frac{k}{\varepsilon}, \quad S = \sqrt{2 S_{ij} S_{ij}}$$

In these equations, G_k is the turbulent kinetic energy due to the laminar velocity gradient, G_b is the turbulent kinetic energy due to buoyancy, and Y_M is the diffusive kinetic energy due to compressible turbulence. C_2 and $C_{1\varepsilon}$ are constants. σ_k and σ_ε are the turbulent Prandtl numbers for k and ε , respectively.

The values of the parameters taken during the simulation are listed in Table 1.

The species transport equation is as follows (Nan 2015):

$$\frac{\partial}{\partial t}(\rho Y_i) + \nabla \cdot (\rho \bar{v} Y_i) = -\nabla \cdot \bar{J}_i + R_i + S_i \quad (6)$$

where Y_i is the local mass fraction of each species; R_i is the net rate of production of species by chemical reaction; S_i is the rate of creation by addition from the dispersed phase plus any defined sources; and \bar{J}_i is the diffusion flux of species i , which arises due to gradients of concentration and temperature.

Description of the shaft model and boundary conditions

Figure 2 shows the model of the ventilation system in the shaft excavation. The net section diameter d of the shaft is 5.5 m, using two $\Phi 600$ -mm diameter flexible duct for ventilation, ducts against the wall arrangement, the shaft depth is taken as 500 m.

The assumptions for the ventilation model are as follows:

- (1) The airflow ejected from the duct is isothermal, uniformly distributed at the outlet and perpendicular to the boundary;
- (2) Harmful gases produced by blasting are thrown within a certain distance near the working face, which is defined as the throwing fume zone, i.e., Area I. After a certain period of time, CO is uniformly distributed in Area I, at this time, the CO concentration in Area I is the initial concentration when the calculation is carried out;
- (3) The gases in the simulation are incompressible;



Table 1 Parameters of the Realizable $k-\epsilon$ turbulence model

$C_{\epsilon 1}$	C_2	$C_{\epsilon 3}$	σ_k	σ_ϵ	S_c	P_{re}	P_{rt}
1.44	1.9	0	1.0	1.2	0.7	0.85	0.85

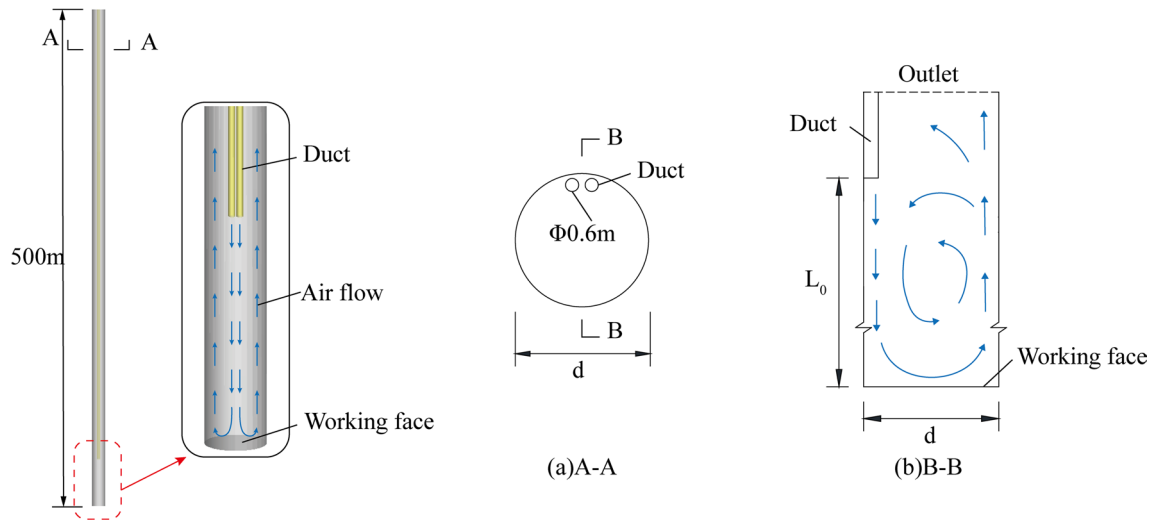


Fig. 2 Schematic diagram of ventilation model

- (4) In this study, the walls of the well are adiabatic, and the temperature of the gas in the wellbore does not change during ventilation.

Based on the actual construction site conditions, the boundary conditions were determined as follows:

- (1) *Inlet boundary conditions:* The fresh airflow is ejected from the outlet of the duct, so the inlet boundary of the model is the outlet of the duct, which is the velocity inlet boundary and can be calculated by Eq. (7).

$$u_{in} = \frac{Q}{S} \tag{7}$$

- (2) *Outlet boundary conditions:* The gases in the shaft are discharged from the outlet of the shaft, so the outlet of the shaft is the outlet boundary. Since the actual engineering shaft is connected with the atmosphere, so the pressure outlet boundary condition is used.
- (3) *Wall boundary conditions:* All walls are defined as fixed wall boundary conditions without slip, while ignoring the thermal boundary conditions of the walls and using the standard wall function method. The boundary of the fluid computational domain uses a wall function method that takes into account the effect of roughness (Lacasse et al. 2004).
- (4) *Initial conditions:* When the project is excavated using the drill and blast method, the harmful gases produced

are mainly carbon monoxide, which can be determined by the following formula (Chang et al. 2020):

$$C_0 = \frac{Gb}{lS} \tag{8}$$

where C_0 is the initial concentration of CO (kg/m^3); G is the amount of explosives required for tunnel blasting (kg); b is the amount of harmful gas produced by 1 kg of explosives (m^3/kg); and l is the throwing length of blasting fume (m), $l = 15 + \frac{G}{5}$ (Nan 2015). S is the area of the cross-section (m^2).

The commercial computational fluid dynamics (CFD) software FLUENT gives reasonable and effective solutions for the above models, so it is chosen for numerical calculations.

In order to study the influence of different factors on ventilation during the construction period of the shaft, 16 different working conditions were divided according to Table 2, and the influence laws of the position of the duct, the distance L_0 between the duct opening and the working face, the air velocity v_0 , and the diameter d of the shaft were investigated, respectively. The most obvious influence on the flow field distribution in the shaft is the location of the ducts, so three arrangements are classified, namely, two ducts arranged side by side, arranged in opposition to each other and arranged at a certain distance from each other. In this way, the mechanism and degree of influence of this factor on the flow field are investigated. The distance L_0 between the outlet of the duct and the working face is

Table 2 Parameters of the shafts in different cases

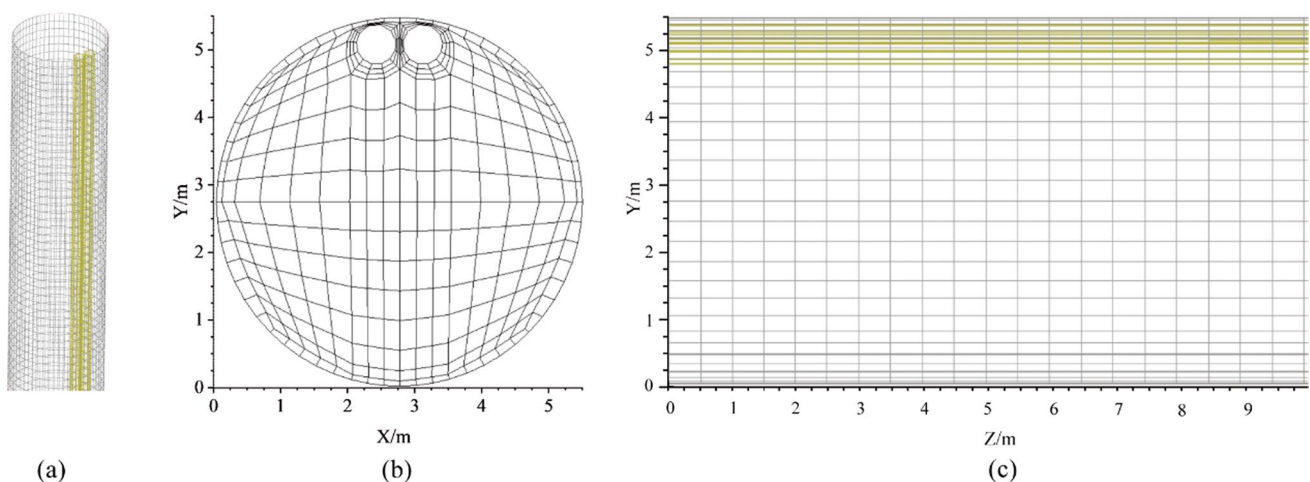
Case		Shaft length (m)	Location of the vent duct	L_0 (m)	v_0 (m/s)	d (m)
C1	C1.1	500	Abreast	20	25	5.5
	C1.2	500	Opposite	20	25	5.5
	C1.3	500	90°	20	25	5.5
C2	C2.1	500	Abreast	20	25	5.5
	C2.2	500	Abreast	25	25	5.5
	C2.3	500	Abreast	30	25	5.5
	C2.4	500	Abreast	35	25	5.5
	C2.5	500	Abreast	40	25	5.5
C3	C3.1	500	Abreast	20	15	5.5
	C3.2	500	Abreast	20	25	5.5
	C3.3	500	Abreast	20	35	5.5
	C3.4	500	Abreast	20	45	5.5
C4	C4.1	500	Abreast	20	25	5.5
	C4.2	500	Abreast	20	25	6.5
	C4.3	500	Abreast	20	25	7.5
	C4.4	500	Abreast	20	25	8.5

selected within the range of the calculated smoke throwing distance when using electric detonator blasting. From the empirical formula, $L_0 \geq (4 \sim 5)\sqrt{S}$, where S is the area of the shaft cross-section (Zheng 2014). The air velocity of ventilation is mainly determined by the ventilation volume Q and duct cross-sectional area S . The ventilation volume is reasonably determined with the actual needs of the project, such as the amount of air required by the staff, the amount of air required by the blasting machinery, the amount of air required for smoke exhaust, and the amount of air required to meet the minimum air velocity in the shaft.

Discussion of grid independence

Figure 3 shows the schematic diagram of the vertical shaft model meshing. As shown in Fig. 3b, the grid is structured, and the grid around the duct is refined and divided by the O-Block method.

The independence of the grid has a great influence on the accuracy of the numerical simulation results (Grönman et al. 2018). In this study, the grid convergence index method (Zhang et al. 2020) was used to verify the grid independence. The more detailed the grid is divided, the more accurate the calculation of the numerical simulation will be, and also the smaller the GCI index will be. In this section, a shaft with a length of 100 m is selected for the study. The ICEM software is used to divide the structured grid with

**Fig. 3** Schematic diagram of grid division

three different grid scales, containing 189,548, 61,392, and 37,234 grids, respectively.

The grid convergence index can be obtained by the following equation (Zhang et al. 2020):

$$GCI_{i+1,i}^{fine} = \frac{F_s e_a^{i+1,i}}{r_{i+1,i}^p - 1} \times 100\% \tag{9}$$

where F_s is the safety factor, taken as 1.25; and e is the relative difference of numerical solutions at different grid scales $e_a^{i+1,i} = |(f_i - f_{i-1})/f_i|$. $r_{i+1,i}$ is the grid refinement factor, which can be obtained by $r_{i+1,i} = h_i/h_{i+1}$. h_i is the grid scale of the i th grid, $i = 1, 2$. p is the convergence accuracy; and f_i is the average flow velocity v on the i th grid at different height (z) sections from the bottom of the shaft.

The convergence of the grid is also evaluated by the convergence ratio R (Zhang et al. 2020).

$$R = \frac{f_2 - f_1}{f_3 - f_2} \tag{10}$$

When $0 < R < 1$, the numerical solution converges monotonically; when $R < 0$. The numerical solution oscillates and converges; when $R > 1$, the numerical solution diverges (Zhang et al. 2020).

To discriminate whether the numerical results are reasonable, the asymptotic domain index β is used to assist in the discrimination. The β in Eq. (11) should be approximated as 1.0.

$$\beta = \frac{r_{21}^p GCI_{21}^{fine}}{GCI_{32}^{fine}} \tag{11}$$

Table 3 presents the evaluation results of the independence analysis of the grid using the GCI method.

From Table 3, it can be seen that the numerical solutions of the three grids oscillate and converge in the range from 0 to 18 m from the bottom of the shaft, and converge

monotonically in the range after 18 m. The calculated values of $e_a^{i+1,i}$ and GCI for the numerical results decrease as the grid is progressively encrypted, indicating that the dependence of the numerical solution on the grid is significantly reduced. The maximum $e_a^{i+1,i}$ of the average flow velocities on different sections of grid 3 and grid 2 is 0.319, and the maximum dispersion is 13.969%, which is a large error, indicating that the error can be effectively reduced by continuing to encrypt the grid on the basis of grid 3. The maximum $e_a^{i+1,i}$ of grid 2 and grid 1 is 0.086, and the maximum dispersion is 3.663%, indicating that the numerical solution of grid 2 is close to the analytical solution. At the same time, the computational asymptotic domain index β is close to 1, which means that the numerical solutions of different cross-sectional flow velocities are already in the asymptotic domain of the analytical solution. Combined with the above analysis, the density of grid 2 has basically met the calculation requirements, and further encryption of the grid has limited improvement on the calculation accuracy. The number of grids will increase exponentially when the grid is encrypted, which will significantly increase the computational time. Therefore, grid 2 is chosen for further analysis and calculation.

Model validation

During the construction of the shaft, the ducts are generally installed close to the wall. Therefore, it is a wall-mounted jet. Nan (2015) conducted an experimental study on a series of three-dimensional advective wall jets in semi-infinite space, so their experimental results on a circular orifice jet model were selected for this study to validate the model. A three-dimensional circular orifice attached wall jet model in semi-infinite space is established based on their experiments. The diameter of the circular outlet is 0.00953 m, and the jet outflow velocity is 7.42 m/s. The notation of a three-dimensional circular wall jet is shown in Fig. 4.

Table 3 Estimation of discretization errors using the GCI method

Z (m)	f_1 (m/s)	f_2 (m/s)	f_3 (m/s)	R	e_a^{32}	e_a^{21}	GCI ₃₂ (%)	GCI ₂₁ (%)	β
2	2.377	2.300	2.534	-0.329	0.102	0.032	7.443	1.144	0.958
6	2.476	2.365	2.596	-0.481	0.098	0.045	13.969	3.514	0.953
10	2.400	2.319	2.466	-0.551	0.063	0.034	12.070	3.663	0.953
14	2.298	2.327	2.222	-0.276	0.045	0.013	2.552	0.324	0.945
18	1.740	2.238	1.525	-0.698	0.319	0.086	7.619	0.238	0.950
25	0.541	0.535	0.511	0.265	0.044	0.011	1.659	0.176	0.970
35	0.328	0.325	0.314	0.318	0.033	0.010	1.522	0.205	0.986
45	0.317	0.321	0.311	-0.385	0.030	0.012	2.848	0.567	0.911
60	0.295	0.293	0.286	0.187	0.026	0.005	0.646	0.042	0.985
75	0.295	0.291	0.284	0.672	0.022	0.015	2.933	1.053	0.980
90	0.291	0.289	0.283	0.279	0.021	0.006	0.837	0.095	0.988

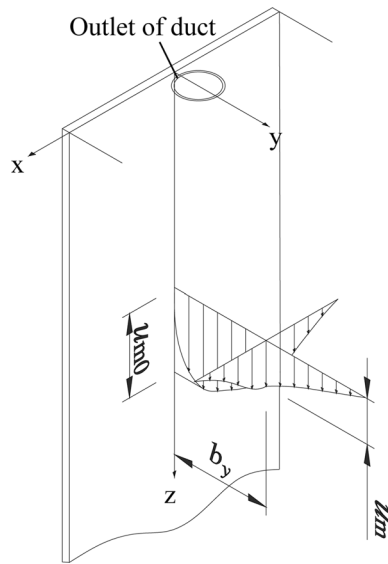


Fig. 4 Three-dimensional wall jet

Figure 5 shows the simulated values of flow velocity at different height sections of the model Z-axis compared with the measured values, and the data are dimensionless. The experimental and simulated values of the maximum airflow velocity for different cross-sections are essentially the same. Therefore, numerical simulation of advective jets in semi-infinite space using Realizable $k-\epsilon$ model can be performed with high accuracy.

Results and discussion

Analysis of the flow field in the shaft

Figure 6 shows the cloud diagram of the flow field distribution in the shaft under different working conditions of C1. The flow distribution in the shaft is complicated. The jet, backflow, and vortex zones are mixed with each other. When the jet is ejected from the outlet of the duct, the surrounding air is sucked by the jet and flows together with the jet to the working face. This area is the jet zone. And the area of the jet zone gradually increases. Until the jet hits the working face, the flow direction is changed by the restriction of the solid wall. Fresh air mixes with CO and flows along the sidewalls of the shaft toward the outlet of the shaft, and this part of the area is the backflow zone. The vortex zone is sandwiched between the jet zone and the backflow zone. This is due to the fact that part of the backflow is affected by the expansion section of the jet and is recoiled into the jet zone, thus forming a vortex zone.

The analysis of the flow field under different working conditions shows that the most influential factor on the distribution of the flow field in the shaft is the choice of the duct position. Therefore, in this section, the flow field under C1 working conditions is selected for comparative analysis. Figure 6a shows the distribution of the flow field in the shaft under C1.1 working condition. When the ducts are arranged side by side, the jet zone is distributed below the outlet of the ducts, the backflow zone is mainly distributed on the opposite side of the jet zone, and the vortex zone is mainly located between the jet zone and the backflow zone. At the same time, the flow rate near the working face is significantly higher in C1.1 compared to C1.2 and C1.3 conditions. This is certainly beneficial to the dilution and emission of CO near the working face. Figure 6b shows the cloud diagram of the flow field in the shaft under C1.2. The jet zone is located at the lower side of the duct outlet. The airflow from both sides of the duct changes direction as it passes through the work face, converges at the 4–4 cross-section, and then flows toward the outlet of the shaft. Influenced by the jet zone, the backflow zone is mainly distributed on both sides near the shaft wall. Figure 6c shows the flow field distribution in the shaft under C1.3 working condition. The distribution of jet zone and backflow zone under this case is more complicated. The length of the jet zone is significantly smaller than the other two working conditions due to the effect of duct jet hedging. The backflow zone is mainly distributed at the position opposite to the duct. The flow velocity of the gas near the working face of the shaft is smaller, which is not conducive to the rapid emission of CO.

The process of forced ventilation is mainly about the dilution and discharge of CO. The jet mainly dilutes CO and the backflow mainly discharges it. In order to further analyze the influence of duct location on the distribution of jet and backflow zones, the size of the jet and backflow zones under different working conditions of C1 was studied. Figure 7 shows the comparison of the area of the jet zone and the area of the backflow zone under different working conditions of C1. The area of the backflow zone is significantly larger than the area of the jet zone under all three working conditions, so all of them can play a good role in the exhaust of CO. The outlet of the duct is located 20 m from the working face of the shaft, so there are obvious fluctuations in the curves of the three working conditions here. The area of the jet zone drops to 0 at 26 m from the working face for C1.2, while it drops to 0 at about 32 m from the working face for C1.1 and at about 37 m from the working face for C1.3. Moreover, the area of the backflow zone is much larger for C1.2 than for the other two conditions in the range of 15 m–30 m from the working face of the shaft. This indicates that the removal of carbon monoxide is more effective when the ducts are arranged relative to each other.



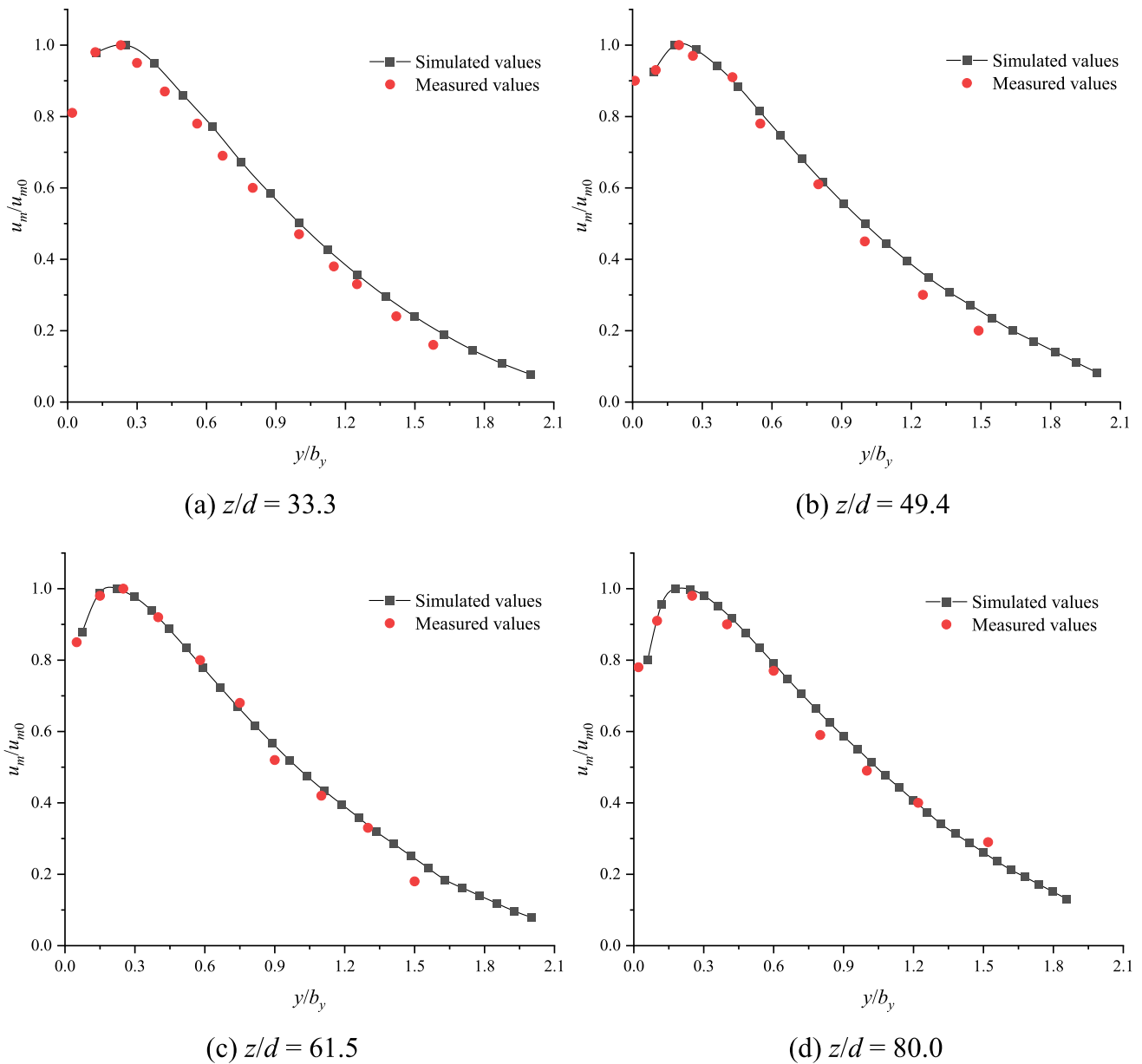


Fig. 5 Comparison of simulated and measured values of flow velocity at different locations

As shown in Fig. 7, the jet zone between 20 and 23 m for C1.2 working condition is mainly located in the area between the two ducts. This is the result of the backflow from the bottom to the top being obstructed by the air above and changing the flow direction again to the bottom of the shaft. The jet zone within the range of 23~26 m is mainly located between the duct and the wall of the shaft. The jet velocity at the outlet of the duct is too fast, causing a negative pressure zone between the outlet of the duct and the wall

of the shaft, thus causing airflow to the working face. In the range of 20~35 m, the area of the jet zone in C1.1 working condition is larger than that of the jet zone in C1.2 working condition. This is because the ducts in C1.1 are arranged side by side, and the jet effect is stronger, so the location where the backflow occurs is farther than that in C1.2. The fluctuation in C1.3 condition at 15 m from the working face of the shaft indicates that the flow field changes here, and

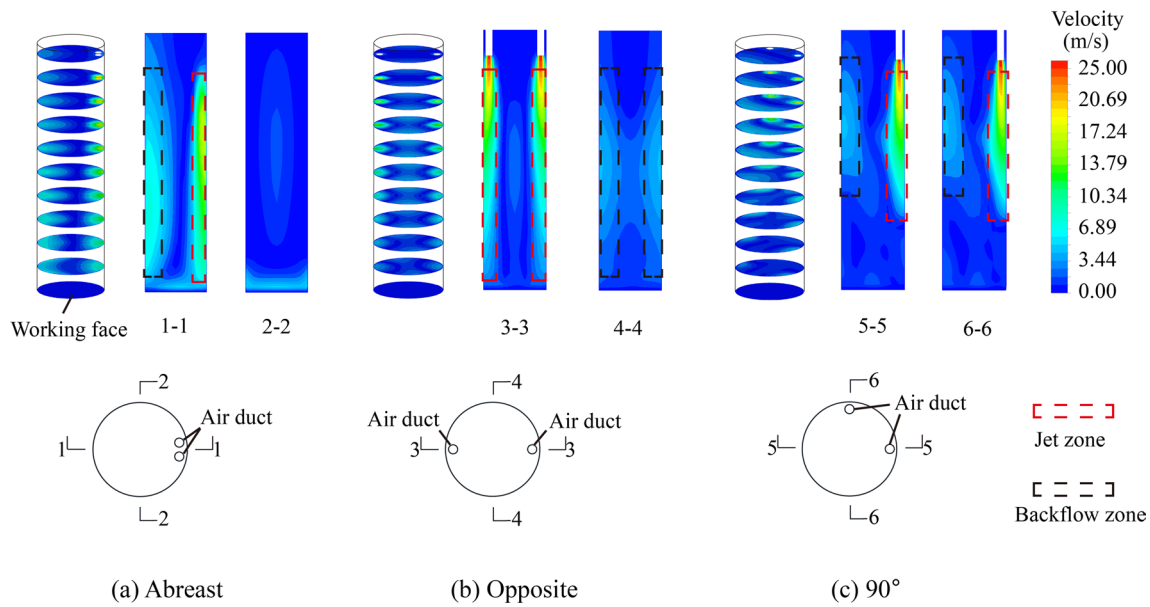


Fig. 6 Cloud diagram of the flow field distribution in the shaft when the air duct is in different positions

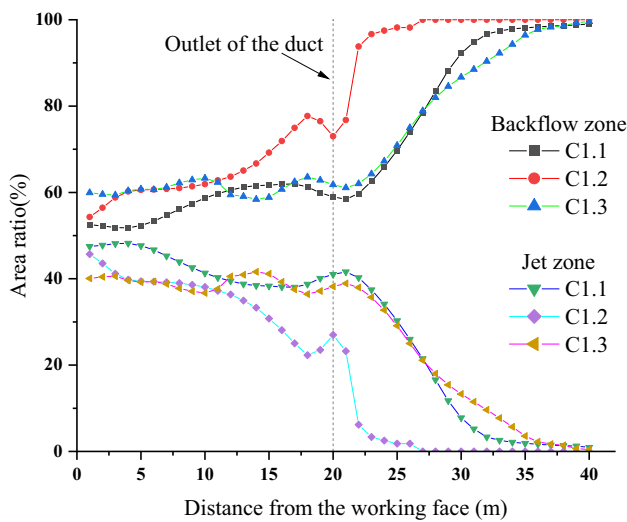


Fig. 7 Comparison of the area for the jet zone and the area for the backflow zone under C1 working condition

the vortex zone is easily formed, which is not conducive to the emission of CO near the working face.

Figure 8 shows the velocity vector distribution of the flow field in Area I. The distribution of the vortex zone inside the shaft under three different working conditions can be seen more intuitively. When the ducts are arranged side by side, the vortex zone is mainly located in the middle of Area I, which is about 15 m. Under C1.2 working condition, it is influenced by the hedging effect of the two duct jets. The vortex zone is located primarily on either side of Sect. 4–4 (Fig. 6). Combined with Fig. 6b, it can be seen

that the distribution of the vortex zone is smaller in this working condition. Therefore, the retention effect is weaker for CO. Under C1.3 working condition, there are obvious vortex zones in many places such as near the working face of the shaft and near the outlet of the duct. The distribution of vortex zone is confusing, which will seriously affect the jet zone and backflow zone, and has a greater impact on the air velocity. It takes 240 s for Area I to reach the safe concentration index for C1.1, 200 s for C1.2, and 270 s for C1.3, which indicates that the presence of the vortex zone has a significant effect on the ventilation time. The larger distribution area of the vortex zone, the longer ventilation time required; the more chaotic distribution of the vortex zone, the longer ventilation time required.

Analysis of CO concentration fields

The condition for construction workers to enter the vicinity of the working face is that the concentration of CO must not exceed 30 mg/m^3 . In order to study the influence of different factors on the emission time of CO, the concentration of CO in different sections was selected for analysis. Figure 9a shows the relationship between CO concentration and time in the outlet section of Area I. Under C1, C3, and C4 conditions, the peaks of CO concentration do not differ much. When the distance L_0 between the outlet of the duct and the working face of the shaft is changed (C2), the peaks of CO concentration show obvious differences. As the distance L_0 increases, the peak concentration of CO gradually decreases. The time required for the concentration of CO in Area I to reach the safe entry standard increases accordingly, but the increase is

not significant. The biggest influence on the ventilation time is the air velocity of the jet in the duct (C3) and the diameter of the shaft (C4). The greater velocity of the air ejected from the duct, the shorter time required for the concentration of CO in Area I to reach the safety standard. On the contrary, the larger diameter of the shaft, the more time it takes for the concentration of CO in Area I to reach the safety standard. Figure 9b shows the variation of concentration with time at the outlet cross-section of the shaft. When the velocity of the jet in the duct and the diameter of the shaft were varied,

the time required for the CO concentration in the shaft to reach the safety standard also changed significantly. When the velocity of the jet in the duct is higher, the span of the CO peak is shorter, which means that the airflow has a stronger effect on the transport of CO. At the same time, the shorter time is needed for the CO concentration in the whole shaft to reach the standard. When the diameter of the shaft is larger, the rate of CO peak movement is slower, and the span of the peak is also larger. The longer ventilation time is required.

The time required to reach the CO concentration standard at different sections is summarized in Table 4. When the CO concentration in this section reaches the standard, it means that the concentration of CO in the shaft before this section also reaches the standard. In the C2 working conditions, the time required to reach the safe concentration is almost the same throughout the shaft. The rate of CO peak movement also differs little, indicating that the distance between the outlet of the duct and the working face of the shaft has almost no effect on the emission of CO. While in the C3 working conditions, the values of the three variables showed significant differences between the different working conditions. The time required for the whole shaft to reach the safe concentration is about 940 s longer in C3.1 than in C3.2 and only about 190 s longer in C3.3 than in C3.4. Analysis of the data in the table shows that when the duct jet velocity is low, increasing the jet velocity has a great influence on the CO emission in the shaft, and the effect is reduced when the jet velocity is larger.

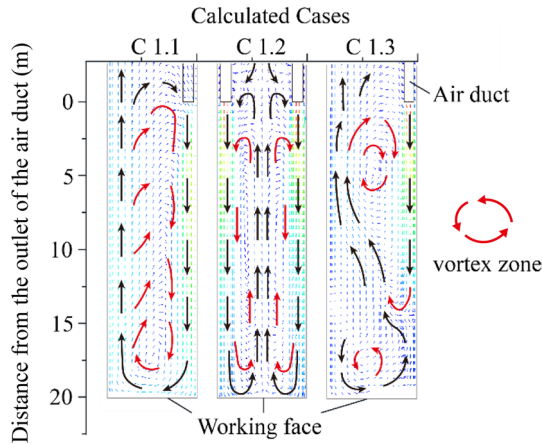
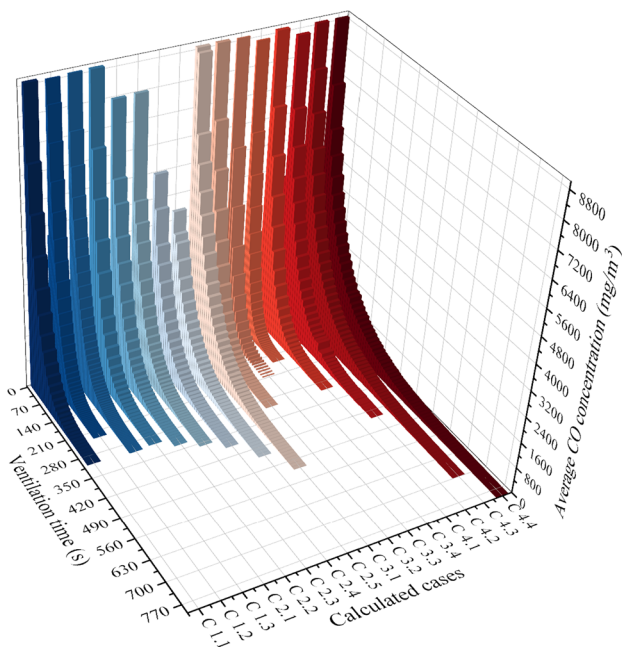
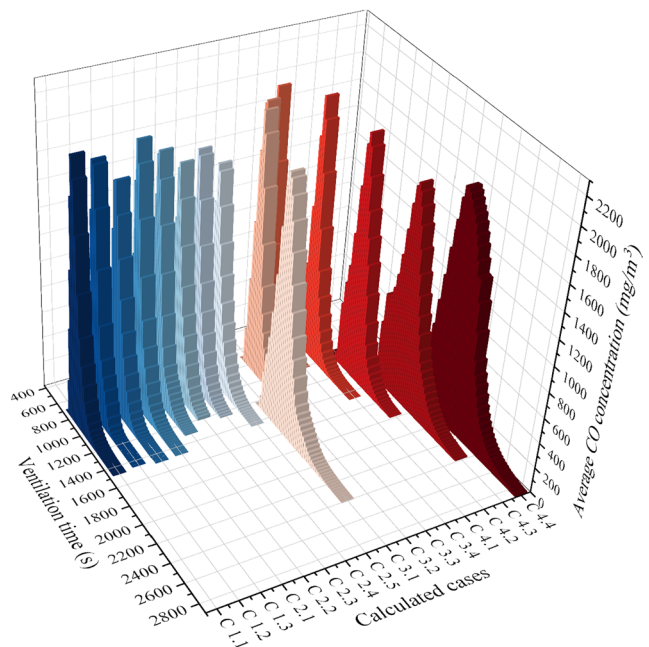


Fig. 8 Flow velocity vector distribution at X=0 section under C1 working condition



(a) Outlet cross-section of Area I



(b) Outlet cross-section of the whole shaft

Fig. 9 Distribution of CO concentration on different cross-sections

Derivation of CO distribution function

When deriving the theoretical distribution function of harmful gases, only the convection process between gases is considered. And according to the results of the above study, there is also a diffusion process of the gas in the process of ventilation. When using the theoretical function for calculation, the peak concentration error of harmful gases is large, and this error becomes larger with the increase in ventilation time. Therefore, in this section, based on the results of the simulated working conditions and considering the convection process of gas as well as the diffusion process, we derive the CO distribution function in the shaft when forced ventilation is used during the construction period of the shaft, and derive the formula for estimating the ventilation time.

Based on the study of the theoretical distribution function of CO in the shaft, the concentration of CO in the shaft is exponentially related to the ventilation time, the ventilation air volume, and the distance of the outlet of the duct from the working face of the shaft. And the laws are the same for different working conditions, so this section takes C1.1 working condition as an example.

Figure 10a shows the dimensionless relationship curve of CO concentration in Area I. C is the concentration of CO at different sections, C_0 is the initial concentration of CO in the shaft, z is the distance between the measurement point and the working face of the shaft, and L_0 is the length of Area I. The values of $\ln(C/C_0)$ for CO at different sections within Area I ($z < L_0$) are almost the same under the same ventilation time, while they are obviously different under different ventilation times. The values of $\ln(C/C_0)$ at different ventilation times are summarized, and the function shown in

Fig. 10b can be obtained. It shows that the value of $\ln(C/C_0)$ for CO inside Area I is not related to the distance from the working face, but is only a function of the ventilation time.

Similarly, the CO concentration in Area II ($z > L_0$) was analyzed by dimensionless analysis. The distribution of CO in Area II is complicated, so the CO emission process is divided into two stages: Before the peak CO concentration is discharged from the outlet of the shaft ($t < T_0$) and after the peak CO concentration is discharged from the outlet of the shaft ($t > T_0$), and T_0 is the time when the peak CO leaves the shaft outlet. The distribution of CO in the shaft at different times is analyzed, again using the C1.1 working condition as an example. Figure 11 shows the distribution of CO along the shaft at different times in Area II under the C1.1 working condition.

Figure 11a reflects the variation of $\ln(C/C_0)$ values for CO with ventilation time at different locations inside the shaft when $t < T_0$. At the same ventilation time, the $\ln(C/C_0)$ values of CO at different sections inside the shaft are different, which can be approximated as a cubic equation of unity about z/L_0 . The difference of the curves is more obvious at different ventilation times. This indicates that the value of $\ln(C/C_0)$ for CO is a function of the distance from the working face and the ventilation time in Area II. Figure 11b shows the dimensionless relationship curve of CO concentration in the shaft after the peak of CO concentration exits the outlet of the shaft ($t > T_0$). The value of $\ln(C/C_0)$ for CO in Area II at the same ventilation time is a primary function of z/L_0 . The coefficients of the primary function are different for different ventilation times. It means that within Area II, the value of $\ln(C/C_0)$ for CO is a function of the distance from the working face and the ventilation time. The $\ln(C/C_0)$

Table 4 Calculation results of different cases

Case	Time to reach safe concentration in Area I (s)	Time for the entire shaft to reach safe concentration (s)	Moving rate of CO peak (m/s)
C1.1	260	1240	0.5852
C1.2	200	1150	0.5898
C1.3	270	1210	0.5863
C2.1	260	1240	0.5852
C2.2	282	1251	0.5882
C2.3	320	1250	0.5882
C2.4	330	1210	0.6167
C2.5	380	1240	0.5852
C3.1	445	2180	0.375
C3.2	260	1240	0.5852
C3.3	180	870	0.8333
C3.4	145	680	1.0417
C4.1	260	1240	0.5852
C4.2	380	1700	0.4583
C4.3	590	2340	0.3758
C4.4	670	2800	0.3333

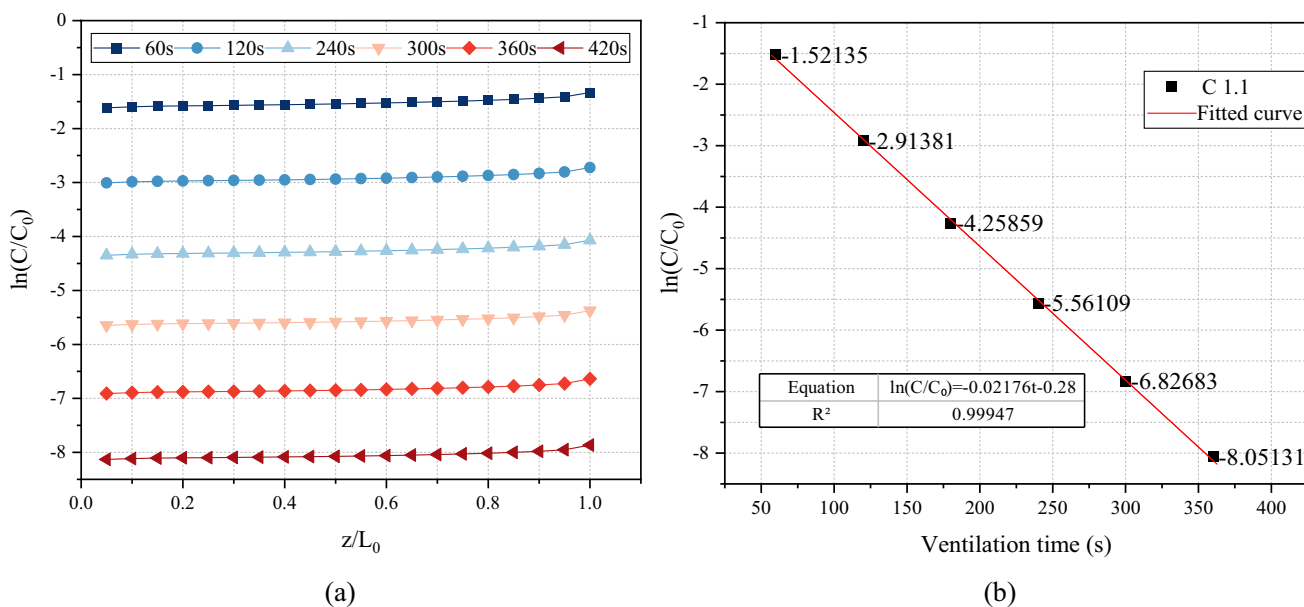


Fig. 10 Distribution of $\ln(C/C_0)$ values for CO in the shaft under C1.1 case: **a** $\ln(C/C_0)$ values at different locations inside the Area I and **b** distribution of $\ln(C/C_0)$ values at different ventilation times

values at different times are comprehensively organized to obtain the surface function of $\ln(C/C_0)$ with respect to

position z and time t . Table 5 summarizes the fitted CO curves for the C1.1 case at different time periods.

Solving the function relationship of the coefficients in the table, the final distribution function of CO in the shaft under C1.1 working case can be obtained as shown in Eq. (12).

$$\ln(C/C_0) = \begin{cases} 0.02176t - 0.286 & z \leq L_0 \\ -0.0195t - 1.2451 + (0.0276t + 2.5947)(z/L_0) & z > L_0, t < T_0 \\ +(-0.1014t + 75.835)(z/L_0)^2 + (0.1356t - 112.04)(z/L_0)^3 & z > L_0, t > T_0 \\ 0.035z - 0.01547t - 3.60743 & \end{cases} \quad (12)$$

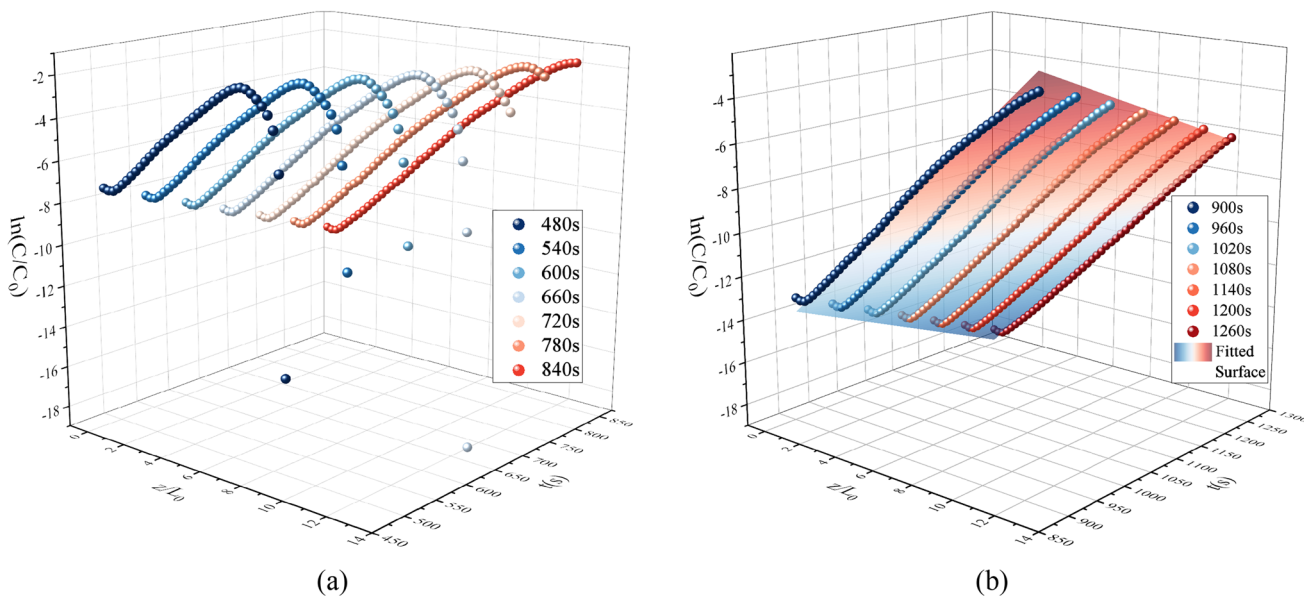


Fig. 11 CO concentration distribution curve and distribution function fitting curve in Area II under C1.1 case

Table 5 Parameters of CO distribution function in the shaft at different times for C1.1 case

$z < L_0$			$z > L_0, t < T_0$		
$t(s)$	Fitted equations	R^2	$t(s)$	Fitted equations	R^2
60	$\ln(C/C_0) = -1.521$	0.9911	480	$\ln(C/C_0) = -10.67 + 16.318(z/L_0) + 28.022(z/L_0)^2 - 51.693(z/L_0)^3$	0.9868
120	$\ln(C/C_0) = -2.913$	0.9933	540	$\ln(C/C_0) = -11.808 + 18.522(z/L_0) + 17.299(z/L_0)^2 - 34.795(z/L_0)^3$	0.9837
180	$\ln(C/C_0) = -4.258$	0.9959	600	$\ln(C/C_0) = -12.898 + 19.463(z/L_0) + 12.784(z/L_0)^2 - 26.529(z/L_0)^3$	0.9825
240	$\ln(C/C_0) = -5.561$	0.9993	660	$\ln(C/C_0) = -14.002 + 19.782(z/L_0) + 11.222(z/L_0)^2 - 22.151(z/L_0)^3$	0.9827
300	$\ln(C/C_0) = -6.826$	0.9923	720	$\ln(C/C_0) = -15.038 + 19.286(z/L_0) + 11.747(z/L_0)^2 - 19.873(z/L_0)^3$	0.9837
360	$\ln(C/C_0) = -8.051$	0.9993	780	$\ln(C/C_0) = -16.475 + 24.825(z/L_0) + 5.195(z/L_0)^2 - 5.051(z/L_0)^3$	0.9947
			840	$\ln(C/C_0) = -17.746 + 27.653(z/L_0) + 13.408(z/L_0)^2 - 2.177(z/L_0)^3$	0.9976

The same treatment is done and analyzed for the rest of each case, and the same law is found. Therefore, when the ducts are arranged close to the wall of the shaft, the distribution function of CO concentration inside the shaft can be expressed by Eq. (13), which is for the distribution of harmful gas concentration inside a single shaft during the construction of the positive shaft method, without branch tunnels and other structures that have an impact on the ventilation of the shaft, ignoring the changes in the temperature of the shaft wall and other pollution sources.

$$C(z, t) = \begin{cases} C_0 e^{a_1 t + a_0} & z \leq L_0 \\ C_0 e^{(b_{01} t + b_{02}) + (b_{11} t + b_{12})(z/L_0) + (b_{21} t + b_{22})(z/L_0)^2 + (b_{31} t + b_{32} t^2)(z/L_0)^3} & z > L_0, t < T_0 \\ C_0 e^{D_0 z + D_1 t + D_2} & z > L_0, t > T_0 \end{cases} \quad (13)$$

where C is the concentration of CO in the shaft (mg/m^3); C_0 is the initial concentration of CO in the shaft (mg/m^3); z is the distance between the measurement point and the working face of the shaft (m); t is the ventilation time (s); L_0 is the distance between the duct opening and the working face of the shaft (m); T_0 is the time required for the CO peak to leave the shaft outlet (s), $T_0 = L/v$; L is the depth of the shaft (m); and v is the velocity at which the CO peak moves, which can be found by the formula summarized from the data in Table 4, $v = 0.2468Q/S - 0.0021$. $a_0, a_1, b_{01} \sim b_{32}$, and $D_0 \sim D_2$ are fitting parameters, which can be calculated by the formula obtained after summarizing the above calculation conditions (see Table 9 for the calculation formula).

To obtain the fitting parameters, the fitted data for the remaining working conditions for different well sections are summarized. Table 6 summarizes the fitted parameters for different working conditions at $z < L_0$.

Table 7 summarizes the fitted parameters for different working conditions at $z > L_0, t < T_0$.

Similarly, the fitting equations for each working condition in the cases of $z > L_0, t > T_0$ can be obtained. Table 8 summarizes the fitting parameters for different working conditions in the cases of $z > L_0, t > T_0$ and the expressions of $D_0 \sim D_1$.

Therefore, the above data were organized to derive several formulas for the fitting coefficients, which are listed in Table 9. In Table 9, Q is the ventilation volume of the fan per unit time (m^3/s); V is the volume of Area I (m^3); and L_0

is the distance between the duct opening and the working face of the shaft (m).

From Eq. (13) fitted above, the empirical equation Eq. (14) can be derived for the ventilation time required to achieve the CO concentration in the shaft during the construction of the positive shaft method.

$$t = \frac{\ln \frac{C_s}{C_0} - D_0 z - D_2}{D_1} \quad (14)$$

where t is the time required to ventilate the whole shaft (s), $D_0 \sim D_2$ are the calculation coefficients, which can be obtained from Table 9; and C_s is the concentration of CO when the shaft allows workers to enter (mg/m^3);

Table 6 Fitting parameters for different working conditions at $z < L_0$

$$z < L_0 \ln(C/C_0) = a_1 t + a_0$$

Cases	a_1	a_0	R^2
C1.1	-0.0218	-0.2864	0.9824
C1.2	-0.0302	-0.0113	0.9862
C1.3	-0.0215	-0.2075	0.9735
C2.1	-0.0218	-0.2864	0.9738
C2.2	-0.0193	-0.4217	0.9932
C2.3	-0.0181	-0.367	0.9864
C2.4	-0.0168	-0.3662	0.9861
C2.5	-0.014	-0.5777	0.9924
C3.1	-0.013	-0.164	0.9464
C3.2	-0.0218	-0.2864	0.9823
C3.3	-0.0319	-0.201	0.9827
C3.4	-0.0394	-0.2911	0.9764
C4.1	-0.0218	-0.2864	0.9927
C4.2	-0.0218	-0.2864	0.9682
C4.3	-0.0302	-0.0113	0.9813
C4.4	-0.0215	-0.2075	0.9953

Verification of the calculation equations

In this study, two engineering examples were selected to validate the obtained formulae for the calculation of ventilation time, which were the Datai shaft of the Wushaoling tunnel (Li and Luo 2005) in China and the No. 2 shaft of the Qinling–ZhongNan Mountain highway tunnel (Xu 2008) in China. Both shafts are forced-ventilated, and the ventilation ducts are arranged against the walls of the shafts. The detailed parameters of each shaft and the required ventilation

time calculated by the equation are listed in Table 10. The actual ventilation times in the table are obtained from field measurements (Li and Luo 2005; Xu 2008). Compared with No. 2 shaft of the Qinling–ZhongNan Mountain highway tunnel, the diameter of Datai shaft is smaller, and the air volume per unit time of the duct is also smaller. And the ventilation time in these two actual projects is judged by the construction personnel through experience, so the time obtained is approximately the same. It can be seen that the error between the time calculated by the derived equation and the actual measured time is within the permissible range. So the time calculation equation derived in this study can be used as a reference for practical engineering projects.

Conclusion

In this study, the process of forced ventilation during the construction period of the shaft was studied by numerical simulation. Different working conditions are determined according to different influencing factors, and by analyzing the flow field as well as the CO concentration field under different conditions, the following conclusions are finally drawn:

- (1) Models were constructed for different operating conditions to investigate the effects of different factors on the flow field and the concentration field of CO in the shaft. The transport process of CO in the shaft is mainly divided into two parts: dilution and diffusion. The vortex zone inside the shaft tends to cause the stag-

Table 7 Fitting parameters for different working conditions at $z > L_0, t < T_0$

$$z > L_0, t > T_0 \ln(C/C_0) = (b_{01}t + b_{02}) + (b_{11}t + b_{12})(z/L_0) + (b_{21}t + b_{22})(z/L_0)^2 + (b_{31}t + b_{32})(z/L_0)^3$$

Cases	b_{01}	b_{02}	b_{11}	b_{12}	b_{21}	b_{22}	b_{31}	b_{32}	R^2
C1.1	-0.0195	-1.2451	0.0276	2.5947	-0.1014	75.835	0.1356	112.04	0.92716
C1.2	-0.0311	1.0624	0.0415	-17.748	-0.2317	225.89	0.3569	-314	0.94263
C1.3	-0.0231	1.0817	0.0304	-11.674	-0.1463	144.03	0.21	-190.77	0.94721
C2.1	-0.0195	-1.2451	0.0276	2.5947	-0.1014	75.835	0.1356	-112.04	0.95125
C2.2	-0.019t	0.3165 +	0.0560	20.527	-0.1989	148.3	0.2193	-174.09	0.95753
C2.3	-0.0206	1.0057	0.0717	-37.352	-0.2397	191.64	0.2442	-200.82	0.99479
C2.4	-0.0192	1.0947	0.0475	-25.624	-0.1898	162.22	0.2215	-185.80	0.9976
C2.5	-0.0158	0.5257	0.0351	-20.534	-0.1492	133.80	0.1772	-152.12	0.99769
C3.1	-0.0150	2.0936	0.0325	-24.367	-0.1030	157.74	0.1050	-165.18	0.99758
C3.2	-0.0195	-1.2451	0.0276	2.595	-0.1014	75.84	0.1356	-112.04	0.99762
C3.3	-0.0333	2.6507	0.0660	-25.216	0.3685	247.22	0.5791	-366.02	0.99813
C3.4	-0.0432	1.4689	0.1062	-28.688	-0.4217	204.19	0.4923	-239.40	0.99869
C4.1	-0.0195	-1.2451	0.0276	2.595	-0.1014	75.84	0.1356	-112.04	0.99848
C4.2	-0.0162	1.0320	0.0238	-16.423	-0.1053	150.38	0.1295	-173.92	0.99848
C4.3	-0.0100	1.0985	0.0203	-20.280	-0.0763	132.50	0.0786	-134.30	0.97690
C4.4	-0.0090	1.4013	0.0208	-28.470	-0.0806	171.46	0.0846	-175.38	0.98758

Table 8 Fitting parameters for different working conditions at $z > L_0, t > T_0$

$z > L_0, t > T_0 \ln(C/C_0) = D_0z + D_1t + D_2$					
Cases	D_0	D_1	D_2	R^2	
C1.1	0.035	-0.0155	-3.6074	0.98716	
C1.2	0.059	-0.0285	-2.4096	0.9981	
C1.3	0.041	-0.0202	-2.0140	0.99694	
C2.1	0.035	-0.0154	-3.6074	0.98716	
C2.2	0.032	-0.0139	-3.4342	0.98128	
C2.3	0.033	-0.0152	-3.0836	0.98568	
C2.4	0.031	-0.0155	-2.151	0.99523	
C2.5	0.025	-0.0136	-1.775	0.99814	
C3.1	0.043	-0.0109	-3.596	0.98861	
C3.2	0.035	-0.0154	-3.6074	0.98716	
C3.3	0.043	-0.0276	-1.5231	0.98947	
C3.4	0.042	-0.0343	-2.681	0.99428	
C4.1	0.035	-0.0154	-3.6074	0.98716	
C4.2	0.041	-0.0136	-3.0238	0.9932	
C4.3	0.03	-0.0083	-1.82	0.99814	
C4.4	0.034	-0.0074	-2.2435	0.99773	
	$D_0 = 0.3022(1/L_0) + 0.0206$	$D_1 = -0.145(Q/V) - 0.0014$	$D_2 = (-4, -1.5)$		

Table 9 Formulas for calculating the coefficients of the fitting formula

Parameter	Calculation function	R^2
a_0	$-0.1821Q/V - 0.0013$	0.9514
a_1	$1.1904Q/V - 0.4546$	0.8908
b_{01}	$-0.1823Q/V - 0.0019$	0.8736
b_{02}	$-41.895Q/V + 3.9064$	0.8039
b_{11}	$0.3716Q/V + 0.0059$	0.8662
b_{12}	$-19.393Q/V - 22.907$	0.8304
b_{21}	$-1.7807Q/V + 0.0068$	0.9661
b_{22}	$267.17Q/V + 121.38$	0.9637
b_{31}	$2.5558Q/V - 0.0462$	0.9635
b_{32}	$-1093.1Q/V - 41.922$	0.9703
D_0	$0.3022(1/L_0) + 0.0206$	0.8760
D_1	$-0.1651Q/V - 0.0017$	0.9661
D_2	$(-4, -1.5)$	-

nation of harmful gases and increase the ventilation time.

- (2) The location of the ducts has a significant effect on the distribution of the flow field in the shaft. When two ducts are used for ventilation and the ducts are arranged in opposition to each other, the area of the backflow zone in the shaft occupies the largest proportion, which is more conducive to the emission of CO. And the distribution of vortex zone is the smallest in

this arrangement. Therefore, the ventilation effect is best in the form of opposing arrangement.

- (3) In the ventilation process, the distance L_0 between the outlet of the duct and the working face has an effect on the size of the CO peak, i.e., on the dilution for CO. The air velocity v of the duct has a great influence on the movement rate of the CO peak. The effect on the diffusion of CO is more obvious than the effect on the dilution of CO. Increasing the air velocity v can effectively shorten the length of the peak CO section, which is more favorable for CO emission. The diameter of the shaft has an effect on the size of the peak as well as the movement rate.
- (4) Based on the theoretical and numerical simulation results, the distribution function of CO concentration in the shaft was derived, and the theoretically derived CO distribution function was supplemented and improved. The empirical formula for calculating the ventilation time required for the shaft construction was also derived and verified by the actual project.

When the internal space of the shaft meets the requirements and the forced ventilation is used, the ventilation can be carried out in the form of double ducts arranged in opposition to each other, which can effectively enhance the dilution effect on harmful gases. At the same time, the distribution law of flow and concentration fields in the shaft, the

Table 10 Comparison for actual ventilation time of the project and the time calculated by the derived formula

Parameter	Datai shaft of the Wushaoling tunnel	No. 2 shaft of the Qinling–ZhongNan Mountain highway tunnel
Depth of the shaft (m)	515.66	660
Diameter of the shaft (m)	5.5	11
Distance between the outlet of the duct and the working face of the shaft (m)	25	20
Ventilation volume of the fan (m ³ /min)	275	648.96
Diameter of the duct (m)	1.2 × 2	0.9
Actual time used for ventilation (min)	30	30
The ventilation time obtained from the equation (min)	(24.48 ~ 27.67)	(25.87 ~ 28.36)
Error (%)	7.8% ~ 18.4%	5.5% ~ 13.8%

derived CO distribution function and the calculation formula of ventilation time can be of reference for similar projects.

Acknowledgements The authors would like to thank Xi'an University of Technology, China, for its support to conduct the present research.

Funding This work was supported by the Leadership Talent Project of Shaanxi Province High-Level Talents Special Support Program in Science and Technology Innovation (2017-TZ0097), the National Natural Science Foundation of China (51679197), and the Natural Science Foundation of Shaanxi Province (2017JZ013).

Data availability All data, models, and codes generated or used during the study are provided along with the submitted article.

Declarations

Conflict of interest The authors declare that there is no conflict of interest regarding the publication of this paper.

References

- Chang X (2020) Study on airflow field characteristics and harmful gas migration law under different ventilation methods. Xi'an university of technology
- Chang X et al (2020) Tunnel ventilation during construction and diffusion of hazardous gases studied by numerical simulations. *Build Environ* 177:106902. <https://doi.org/10.1016/j.buildenv.2020.106902>
- Grönman A et al (2018) Experimental and numerical analysis of vaned wind turbine performance and flow phenomena. *Energy* 159:827–841. <https://doi.org/10.1016/j.energy.2018.06.204>
- Guo C et al (2021) Single-channel blowing-in longitudinal ventilation method and its application in the road tunnel. *Tunn Undergr Space Technol* 108:103692. <https://doi.org/10.1016/j.tust.2020.103692>
- Hasheminasab F et al (2019) Numerical simulation of methane distribution in development zones of underground coal mines equipped with auxiliary ventilation. *Tunn Undergr Space Technol* 89:68–77. <https://doi.org/10.1016/j.tust.2019.03.022>
- Huang Y-D et al (2011) Effects of the ventilation duct arrangement and duct geometry on ventilation performance in a subway tunnel. *Tunn Undergr Space Technol* 26(6):725–733. <https://doi.org/10.1016/j.tust.2011.05.005>
- Kazakov BP et al (2015) Stability of natural ventilation mode after main fan stoppage. *Int J Heat Mass Transf* 86:288–293. <https://doi.org/10.1016/j.ijheatmasstransfer.2015.03.004>
- Lacasse D et al (2004) On the judicious use of the k–ε model, wall functions and adaptivity. *Int J Therm Sci* 43(10):925–938. <https://doi.org/10.1016/j.ijthermalsci.2004.03.004>
- Li Y, Luo X (2005) Construction ventilation technique applied in datai vertical shaft of wushaoling tunnel. *Tunnel Constr* 5:61–64
- Liu Z et al (2014) Simulation of construction ventilation in deep diversion tunnels using Euler-Lagrange method. *Comput Fluids* 105:28–38. <https://doi.org/10.1016/j.compfluid.2014.09.016>
- Liu Z et al (2018) Two-phase flow simulation of construction ventilation in the complex diversion tunnels with long vertical shafts. *J Tianjin Univ* 51(11):1139–1146
- Liu Y et al (2019) A network model for natural ventilation simulation in deep buried underground structures. *Build Environ* 153:288–301. <https://doi.org/10.1016/j.buildenv.2019.01.045>
- Nan C (2015) Numerical study on ventilation and smoke discharge for long-distance and complicated underground caverns. Tsinghua University
- Nan C et al (2015) Numerical study on the mean velocity distribution law of air backflow and the effective interaction length of airflow in forced ventilated tunnels. *Tunn Undergr Space Technol* 46:104–110. <https://doi.org/10.1016/j.tust.2014.11.006>
- Parra MT et al (2006) Numerical and experimental analysis of different ventilation systems in deep mines. *Build Environ* 41(2):87–93. <https://doi.org/10.1016/j.buildenv.2005.01.002>
- Peng Y et al (2021) Application of computational fluid dynamics in subway environment without fire and smoke—Literature review. *Build Environ* 206:108408. <https://doi.org/10.1016/j.buildenv.2021.108408>
- Semin M, Levin L (2021) Theoretical study of partially return air flows in vertical mine shafts. *Therm. Sci. Eng. Progr* 23:100884. <https://doi.org/10.1016/j.tsep.2021.100884>
- Shao S et al (2016) Numerical analysis of different ventilation schemes during the construction process of inclined tunnel groups at the Changheba Hydropower Station, China. *Tunn Undergr Space Technol* 59:157–169. <https://doi.org/10.1016/j.tust.2016.07.007>
- Sousa RL, Einstein HH (2021) Lessons from accidents during tunnel construction. *Tunn Undergr Space Technol* 113:103916. <https://doi.org/10.1016/j.tust.2021.103916>
- Szłazak N et al (2017) Analysis of connecting a forcing fan to a multiple fan ventilation network of a real-life mine. *Process Saf Environ Prot* 107:468–479. <https://doi.org/10.1016/j.psep.2017.03.001>
- Tang B et al (2018) Experiences of gripper TBM application in shaft coal mine: a case study in Zhangji coal mine, China. *Tunn*



- Undergr Space Technol 81:660–668. <https://doi.org/10.1016/j.tust.2018.08.055>
- Tangjarusritaratorn T et al (2022) Numerical investigation on arching effect surrounding deep cylindrical shaft during excavation process. *Underground Space* 7(5):944–965. <https://doi.org/10.1016/j.undsp.2022.01.004>
- Toraño J et al (2009) Models of methane behaviour in auxiliary ventilation of underground coal mining. *Int J Coal Geol* 80(1):35–43. <https://doi.org/10.1016/j.coal.2009.07.008>
- Wang X et al (2009) Construction schedule simulation of a diversion tunnel based on the optimized ventilation time. *J Hazard Mater* 165(1):933–943. <https://doi.org/10.1016/j.jhazmat.2008.10.115>
- Wang X et al (2011) Numerical simulation of TBM construction ventilation in a long diversion tunnel. *Tunn Undergr Space Technol* 26(4):560–572. <https://doi.org/10.1016/j.tust.2011.03.001>
- Wang F et al (2012) Numerical study of effects of deflected angles of jet fans on the normal ventilation in a curved tunnel. *Tunn Undergr Space Technol* 31:80–85. <https://doi.org/10.1016/j.tust.2012.04.009>
- Wang Y et al (2022) Study on the utilization of non-mechanical ventilation power in extra-long highway tunnels with shafts. *J Wind Eng Ind Aerodyn* 221:104909. <https://doi.org/10.1016/j.jweia.2022.104909>
- Xie B et al (2018) Numerical study of natural ventilation in urban shallow tunnels: impact of shaft cross section. *Sustain Cities Soc* 42:521–537. <https://doi.org/10.1016/j.scs.2018.07.022>
- Xie Z et al (2021) Numerical study on fine dust pollution characteristics under various ventilation time in metro tunnel after blasting. *Build Environ* 204:108111. <https://doi.org/10.1016/j.buildenv.2021.108111>
- Xu H (2008) Study on optimization for the construction technology of deep shaft with super large diameter. Tongji University
- Yang L et al (2000) Discussion on the calculation of ventilation and smoke exhaust air volume after tunnel construction blasting. *West-China Explor Eng* 1:55–56
- Zhang Z et al (2018) Natural wind utilization in the vertical shaft of a super-long highway tunnel and its energy saving effect. *Build Environ* 145:140–152. <https://doi.org/10.1016/j.buildenv.2018.08.062>
- Zhang H et al (2019) Study on key parameters of using natural ventilation in shaft to assist mechanical ventilation. *Chin J Undergr Space Eng* 15(04):1258–1266
- Zhang H et al (2020) Parameter analysis and performance optimization for the vertical pipe intake-outlet of a pumped hydro energy storage station. *Renew Energy* 162:1499–1518. <https://doi.org/10.1016/j.renene.2020.07.135>
- Zheng S (2014) Research on numerical simulation of regularities of dust distribution of front pumping back pressing hybrid ventilation in machine operating work face. *Taiyuan University of Technology*
- Zhou Y et al (2020) Effect of press-in ventilation technology on pollutant transport in a railway tunnel under construction. *J Clean Prod* 243:118590. <https://doi.org/10.1016/j.jclepro.2019.118590>

Springer Nature or its licensor (e.g. a society or other partner) holds exclusive rights to this article under a publishing agreement with the author(s) or other rightsholder(s); author self-archiving of the accepted manuscript version of this article is solely governed by the terms of such publishing agreement and applicable law.

